RESEARCH ARTICLE | JUNE 27 2012

Nanostructuring of molybdenum and tungsten surfaces by low-energy helium ions

Gregory De Temmerman; Kirill Bystrov; Jakub J. Zielinski; ... et. al

Journal of Vacuum Science & Technology A 30, 041306 (2012)
https://doi.org/10.1116/1.4731196

Nanostructuring of molybdenum and tungsten surfaces by low-energy helium ions

Gregory De Temmerman,[a] Kirill Bystrov, and Jakub J. Zielinski
FOM Institute DIFFER, Ducth Institute For Fundamental Energy Research, Association EURATOM-FOM, Trilateral Euregio Cluster, P.O. Box 1207, 3430 BE Nieuwegein, The Netherlands

Martin Balden and Gabriele Matern
Max Planck Institute for Plasma Physics, EURATOM Association, 85748 Garching, Germany

Cecile Arnas
Laboratoire PIIM, CNRS/Aix-Marseille Universit, 13397 Marseille, France

Laurent Marot
Department of Physics, University of Basel, Basel, CH-4056, Switzerland

(Received 19 April 2012; accepted 7 June 2012; published 27 June 2012)

The formation of metallic nanostructures by exposure of molybdenum and tungsten surfaces to high fluxes of low energy helium ions is studied as a function of the ion energy, plasma exposure time, and surface temperature. Helium plasma exposure leads to the formation of nanoscopic filaments on the surface of both metals. The size of the helium-induced nanostructure increases with increasing surface temperature while the thickness of the modified layer increases with time. In addition, the growth rate of the nanostructured layer also depends on the surface temperature. The size of the nanostructure appears linked with the size of the near-surface voids induced by the low energy ions. The results presented here thus demonstrate that surface processing by low-energy helium ions provides an efficient route for the formation of porous metallic nanostructures. © *2012 American Vacuum Society*. [http://dx.doi.org/10.1116/1.4731196]

I. INTRODUCTION

The paramount importance of nanoparticles and nanostructured surfaces in various fields of material-related research stems from the unique properties of these surfaces. In particular, nanostructured surfaces with large porosities are very beneficial for photo-catalytic processes such as the photo-electrochemical splitting of water, for example.[1,2] In addition, there is a growing interest for the development of black metals, *i.e.*, nanostructured metals allowing maximum light absorption for solar power concentration where refractory metals are of interest because of their high melting points.[3]

Bombardment of metallic surfaces by energetic ions (keV range) is known to lead to strong microstructural changes such as dislocation loops, voids, holes, etc. It has recently been observed that strong morphology changes, such as blister formation, can also occur on metal surfaces when the ion energy is below the threshold for atom displacement.[4] This effect is especially pronounced in the case of low-energy helium ions. Tungsten surfaces exposed to large fluences of low energy (<60 eV) helium ions are found to exhibit a nanostructured surface morphology consisting of nanometric filaments.[5,6] Detailed studies have been conducted to elucidate the formation mechanism of such structures[7,8] which appears linked to the formation and coalescence of helium bubbles in the near-surface region inducing swelling of the surface. The helium-induced nanostructure in these studies is characterized by a very low density of less than 10% of that of the bulk material[9] and hence a high level of porosity causing a total blackening of the surface completely. In turn, the surface reflectivity has been measured[10] to be as low as 1% across the whole visible spectrum, making such surfaces ideal for optimum light absorption. There are some indications that this process is not exclusive to tungsten but that other metals such as molybdenum could be used to produce similar structures.[10]

The present article compares the development of helium-induced nanostructures on molybdenum and tungsten under similar conditions. The evolution of the surface morphology as a function of plasma exposure time, surface temperature, and ion energy will be discussed.

II. EXPERIMENT

Polycrystalline tungsten and molybdenum samples were exposed to pure helium plasmas in the Pilot-PSI linear plasma generator. The plasma is generated by a so-called cascaded arc source and exhausts into the vacuum vessel. An axial magnetic field is used to confine the plasma and generate an intense magnetized cylindrical plasma beam. The experimental setup is described in more detail elsewhere.[11] The magnetic field was fixed at 0.4 T and can be maintained for a duration of 150 s. Discharge currents in the range 150–250 A and gas flows in the range 1.4–2 slm (1 standard liter per minute $= 4.48\times 10^{20}$ part s^{-1}) were used in this study. The plasma parameters are measured by means of a Thomson scattering (TS) system[12] located at a distance of 17 mm from the plasma-exposed surface. The plasma density and temperature exhibit Gaussian profiles with a full-width half maximum (FWHM) of about 10 mm. Plasma densities

[a]Author to whom correspondence should be addressed; electronic mail: g.c.detemmerman@differ.nl

and temperature were in the range 0.4–3 $\times 10^{20}\,m^{-3}$ and 1.3–3 eV, respectively. Figure 1 shows typical profiles of electron densities and temperature during a helium discharge used in the experiments presented here. The ion flux to the surface is determined from the Thomson scattering measurements by assuming that ions are accelerated over the presheath up to the sound speed.[13] In addition, ion fluxes determined from ion saturation current measurements are found to be in good agreement with the TS measurements. The ion fluxes used in this study were in the range $0.7–3 \times 10^{24}\,m^{-2}\,s^{-1}$ or $11–48 \times 10^{4}\,A\,m^{-2}$.

Plasma-exposed samples were made of polycrystalline tungsten and molybdenum cut from a rod. After polishing to a mirror finish, the samples were ultrasonically cleaned in acetone and alcohol, and outgassed at 1000 °C for 15 min. The samples are clamped on a water-cooled copper holder; an intermediate layer of Grafoil is used to improve the thermal contact. Note that the plasma-exposed surface has a diameter of 22 mm which is larger than the FWHM of the plasma beam; hence the surface temperature has a Gaussian profile. The peak surface temperature is measured by a multiwavelength pyrometer (FMPI SpectroPyrometer, FAR Associates) which measures in the wavelength range 900–1600 nm f, while the 2D surface temperature profile is measured by a fast infrared camera (FLIR SC7500MB) with a typical frame rate of 100 Hz. The surface emissivity is determined by cross-calibration with the pyrometer measurements. The pyrometer measures the light emitted from the sample in the range 900–1600 nm. The surface temperature is then determined by a fit of the measured spectrum and a comparison with Planck's curve. The surface emissivity is then determined by comparing the measured photon fluxes to what would be expected from a blackbody. The emissivity value for the infrared camera is then adjusted so that the temperature determined from the IR camera matches that from the pyrometer. In general, the resulting emissivity value is observed to be very close to that determined by the pyrometer. Detailed heat load calculations have shown that this technique yields a good agreement with calorimetric measurements of the plasma-deposited power.[14] The surface temperature is coupled with the plasma-deposited power and is controlled by varying the plasma conditions. Surface temperatures in the range 600–2000 °C were used. After plasma exposure, the samples are analyzed by scanning electron microscopy (SEM), top view and cross-section, and energy dispersive x-ray spectroscopy (EDX). Tungsten samples were analyzed with a Hitachi S-4800 field emission microscope with a 5 kV acceleration voltage. Cross-sectioning of the samples was carried out by mechanical cleavage; the sectioned surface was then observed without further preparation. Molybdenum surfaces were observed using a Helios NanoLab 600 microscope. Cross-sectioning of the samples was done *in situ* using a focused 30 keV gallium ion beam.

III. RESULTS AND DISCUSSION

During plasma exposure the surface temperature is monitored by a spectropyrometer, which allows an *in situ* study of the evolution of the surface emissivity. Figure 2 shows the temporal evolution of the peak surface temperature and emissivity (at the location of the maximum temperature) of a molybdenum and tungsten surface during successive plasma exposures (delimited by dashed lines). In both cases, the initial emissivity is relatively low because of the mirror-finish polishing but increases very fast during the first 50–100 s of

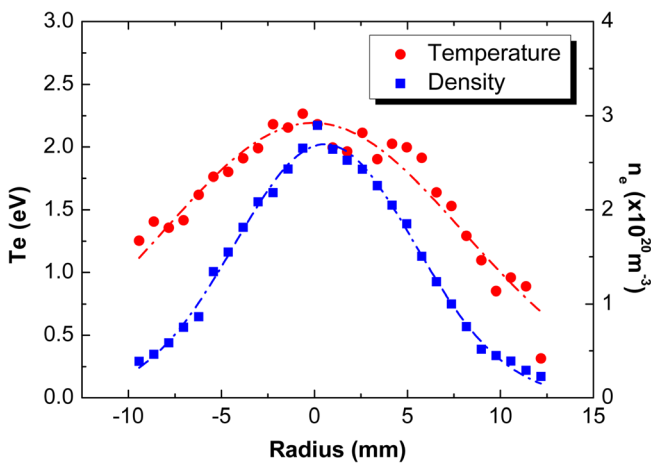

FIG. 1. (Color online) Typical electron temperature (T_e) and density (n_e) profiles of the helium plasmas used during the experiments. The FWHM of the plasma beam is typically 1 cm.

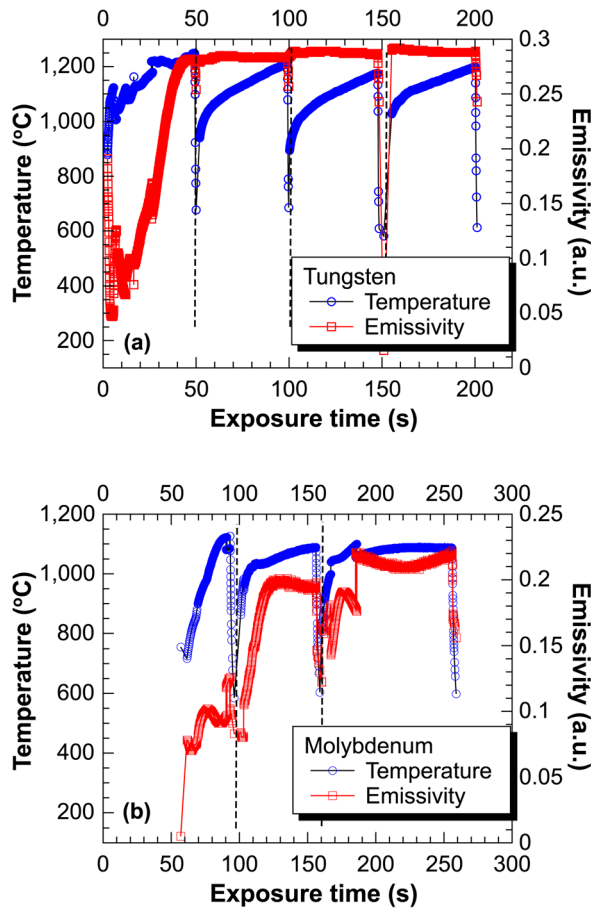

FIG. 2. (Color online) Evolution of the surface temperature and emissivity of (a) tungsten and (b) molybdenum surfaces exposed to high flux helium plasmas ($1 - 2 \times 10^{24} m^{-2} s^{-1}$) with $E_{ion} = 45$ eV.

plasma exposure. In the case of tungsten [Fig. 2(a)], the emissivity increases from 0.07 to 0.29 within the first plasma exposure and remains almost constant during the following exposure. Note that the value of the emissivity is not absolute as it accounts for the optical system transmission and instrument factors. For molybdenum [Fig. 2(b)], only a slight increase of the emissivity is measured during the first plasma pulse but the temperature varies strongly during the pulse; note that the signal was too low during the first 50 s of plasma exposure to get a reliable signal. In the following pulse, the emissivity rises very fast (a factor of 2) within about 20 s and then remains constant during the remainder of the exposure. It is interesting to note that the initial emissivity values during the second exposure correspond to the final emissivity value obtained during the first exposure, indicating an incremental surface modification. The emissivity remains almost constant during the third exposure—the discontinuity in the data between 150 and 180 s is caused by an automatic setting change after saturation of the pyrometer. After exposure, both samples showed a total blackening of the surface. Those observations are consistent with the observed darkening and decreased reflectivity of tungsten surfaces after exposure to pure helium plasmas, which has been reported previously.[6,15,16] The current results demonstrate that the surface blackening occurs on a very short time scale for fluences higher than $10^{25}\,m^{-2}\,s^{-1}$.

Figure 3 shows SEM pictures of molybdenum surfaces after exposure to a helium plasma for 500 s, corresponding to a fluence of $3 \times 10^{26} m^{-2}$, and with a surface temperature of 1000 °C and two different ion energies, 25 and 45 eV. The observed surface modifications strongly depend on the impinging ion energy. For $E_{ion} = 25$ eV, the morphology changes appear to be dependent on the grain orientation as illustrated in Fig. 3(a) where sharp boundaries between different surface structures are clearly observed. Figures 3(b) and 3(c) show high magnification pictures of those different structures. While large pore formation is common to these two areas, the pore shape is very different. Both circular [Fig. 3(b)] and elongated pores [Fig. 3(c)] are visible. In some cases, pinholes can be found at the bottom of the elongated voids. When the ion energy is increased to 45 eV, the surface is covered with nanoscopic filaments whose diameter is in the range 20–50 nm [Fig. 3(d)]. The plasma-exposed surface then appears homogeneous with no signs of the grain-dependent behavior observed at lower ion energy. Figure 4 illustrates the surface modifications induced by high fluxes of low energy helium ions on tungsten substrates with a temperature of 1000 °C. The experimental conditions were similar to those used for the molybdenum samples. Here also, for the lowest ion energy, the appearance of the modified surface is dependent on the tungsten grain orientation [Fig. 4(a)]. In the two cases, many pinholes are observed on the surface with sizes below 50 nm. In Fig. 4(b), irregularly-shaped structures are seen protruding from the surface. In other locations [Fig. 4(c)], a wavy structure is observed also with protruding filaments. It is interesting to note that although the surface modifications in both cases are rather different, the shape of the protrusions in both cases is similar. At higher ion energies, a fully-developed nanostructure is formed [Fig. 4(d)].

The effect of the helium ion energy on the surface modifications of tungsten was investigated in detail in Ref. 17. It was found that below 27 eV surface modifications could hardly be detected (by SEM) while an ion energy of 32–37 eV was necessary to observe the protrusion of a nanostructure from the surface. Similarly, it is reported in Ref. 7 that below 20 eV, only void formation on the surface were observed but that protruding filaments were absent. Our data confirm the strong influence played by the ion energy on the helium-induced surface modification process. It appears that increasing the ion energy from 25–45 eV strongly accelerates the formation rate of the nano-filaments although nano-filament formation is already observed at 25 eV. Ion-produced damages can be excluded since the ion energy in this study is well below the expected threshold (≈ 0.5 keV) for helium on tungsten. An increase of the ion energy from 25–45 eV will modify the ion penetration depth and the particle reflection coefficient, *i.e.*, the helium trapping in the

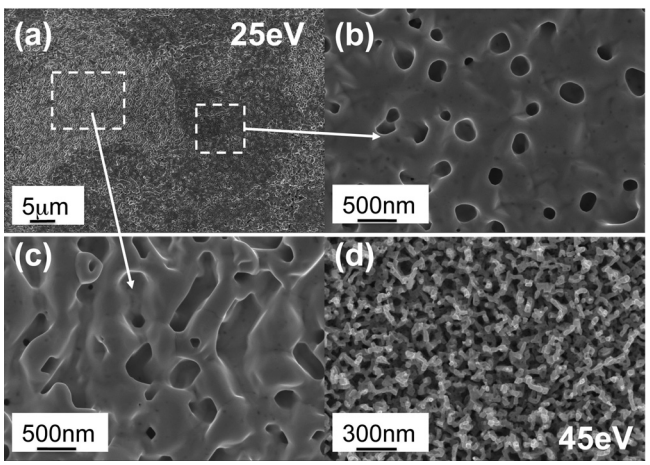

FIG. 3. Surface morphology of molybdenum surfaces induced by helium plasma exposure for a duration of 500 s, with a surface temperature of 1000 °C as a function of the impinging ion energy.

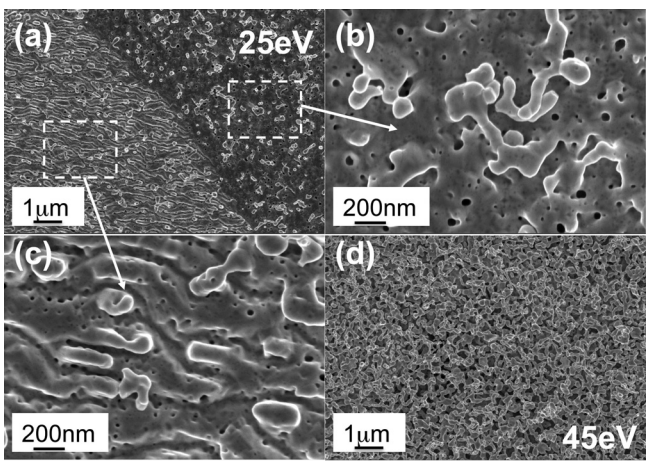

FIG. 4. Surface morphology of tungsten surfaces induced by helium plasma exposure for a duration of 500 s, with a surface temperature of 1000 °C as a function of the impinging ion energy.

surface, which has been experimentally measured in Refs. 17–19. In addition, it has been previously shown[20] that the development rate of helium-induced nanostructures on tungsten increases with the incoming ion flux and saturates for a helium flux of $10^{22}m^{-2}s^{-1}$, implying that a given helium concentration in the near-surface is needed for the morphology changes to occur.

Figure 5 shows the morphology of tungsten surfaces exposed to similar plasma conditions to those in Fig. 4 but with a surface temperature of 1400 °C. Filament protrusion is clearly observed even for the lowest ion energy. A strong surface roughening together with the presence of numerous pinholes can be seen in Figs. 5(a) and 5(b). It is rather remarkable that some of those protrusions appear to be barely attached to the surface. At the same time, some protrusions are forming bridges and/or have bended shapes. In general, the protrusions do not exhibit particular alignment with respect to the surface, which would indicate that the formation process is independent on the electric field present in the electrostatic sheath. The height distribution of the filaments is relatively wide as can be observed from Fig. 5(b). A comparison of Figs. 5(b) and 5(d) points once again to the strong influence of the ion energy on the surface modification kinetics. While at 25 eV the filament height is around 100 nm and the surface coverage relatively low, at 45 eV a full coverage of the surface is obtained and the thickness of the plasma-modified surface is in the range 500–800 nm. The cross-section images [Figs. 5(c) and 5(d)] clearly evidence the presence of large voids in the near-surface region. In addition, voids extending in different directions and with an inner diameter of up to 100 nm can be observed. It therefore appears as if the surface protrusions are related to the surface swelling induced by the growth of the near surface bubbles.[7] The protruding structures appear to present faceted surfaces on their top part [Fig. 5(d)].

The effect of the surface temperature on the helium-induced surface modification is further investigated in Fig. 6 for molybdenum surfaces. In this case, the ion energy was

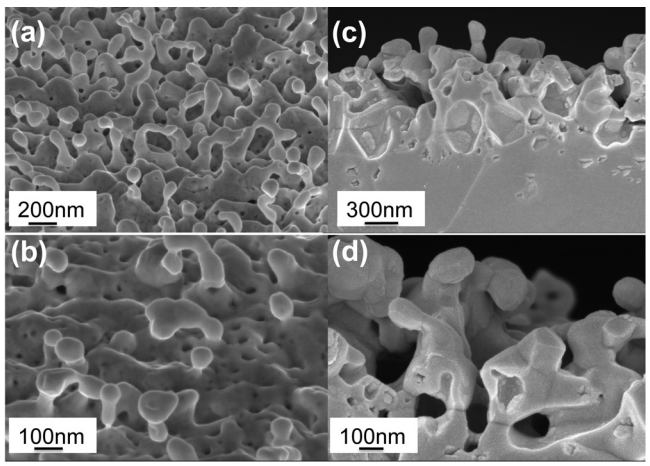

FIG. 5. Scanning electron microscope images of tungsten surface after exposure to a helium fluence of $3 \times 10^{26}m^{-2}$ (500 s) with a surface temperature of 1400 °C, with $E_{ion} = 25$ eV [(a) and (b) with a tilt of 45°] and $E_{ion} = 45$ eV [(c) and (d) cross-section images].

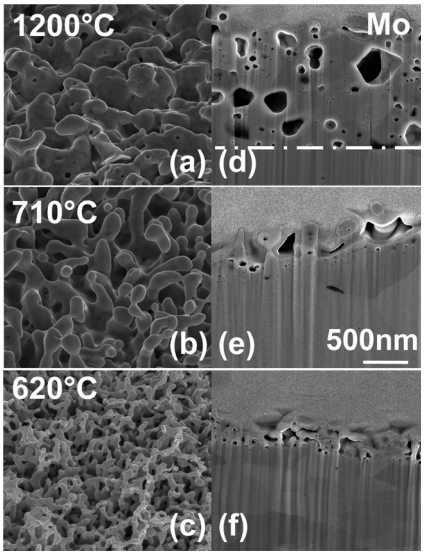

FIG. 6. Evolution of the helium-induced surface morphology changes of molybdenum surfaces as a function of the surface temperature during plasma exposure ($E_{ion} = 45$ eV, t = 1000 s). For each exposure temperature, top-views (tilted by 52°) and cross-sections are shown in the same magnification on the left and right sides, respectively. The dashed line in (d) indicates the boundary between the plasma-modified layer and the unaffected bulk.

45 eV and the exposure time was 1000 s. Both top-view and cross section images are shown. Evidently, the surface temperature has a strong effect on the resulting surface morphology. At 620 °C, the surface is covered by nanoscopic filaments with a diameter lower than 100 nm [Fig. 6(c)]. At 710 °C, the filament size increases to about 200–250 nm, while at 1200 °C a rounded morphology is observed with a characteristic scale around 500 nm. The cross-section images show the presence of voids in the near surface region, the typical size of which increases with the surface temperature. It is interesting to notice that the characteristic dimensions of the surface morphology correlates well with the size of the near-surface voids, confirming that both are linked. The size distribution of the voids is very large and ranges, for the highest temperature, from several nm to 500 nm [Fig. 6(d)]. The voids are inhomogeneously distributed within the sub-surface region. A sharp boundary exists between the plasma-modified area and the undamaged bulk material. The thickness of the plasma-modified zone increases with the surface temperature similarly to the size of the near-surface voids. Figure 7 summarizes the evolution of the thickness of the plasma-modified layer as a function of the surface temperature and plasma exposure time. Since the samples were exposed under similar ion flux conditions, the latter is equivalent to the ion fluence. The nanostructured layer thickness evidently increases with surface temperature and exposure time. A factor of 3 increase of the thickness is observed between 710 °C and 1200 °C. In addition, when the exposure time is doubled (500 and 1000 s), the thickness increases by a factor of 2.2 and 2.7 at 710 °C and 1200 °C, respectively.

Figure 8 illustrates the effect of the surface temperature on the helium-induced morphology changes of tungsten surfaces bombarded by 45 eV helium ions. As for the case of molybdenum surfaces (Fig. 6), there is a strong correlation

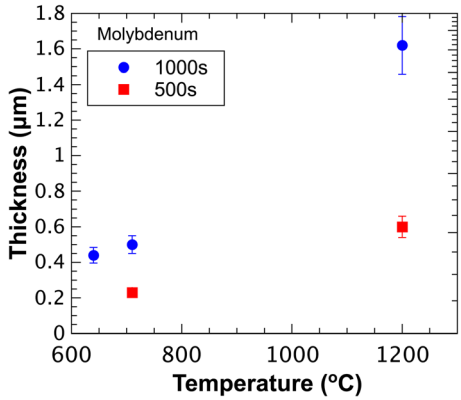

FIG. 7. (Color online) Evolution of the thickness of the plasma-modified sub-surface region as a function of the surface temperature during exposure for molybdenum surfaces. The ion energy was 45 eV, the ion fluence was $4.5 \times 10^{26} m^{-2}$ (500 s) and $9 \times 10^{26} m^{-2}$ (1000 s).

between the surface temperature during plasma exposure and the resulting structure size. At 1000 °C, nanoscopic filaments with a diameter lower than 20 nm are formed. When the temperature is increased to 1500 °C, the structure size is in the range 100–200 nm while micrometric voids are observed on the surface of the sample exposed at 2000 °C. The cross-section images are also consistent with those of the molybdenum samples with an increase in the size of the near-surface voids with surface temperature. It should be mentioned that voids are not visible in the picture shown here for the sample exposed at 1000 °C because of their very small size. As in the case of molybdenum surfaces, a sharp boundary exists between the plasma-modified region and the unaffected bulk.

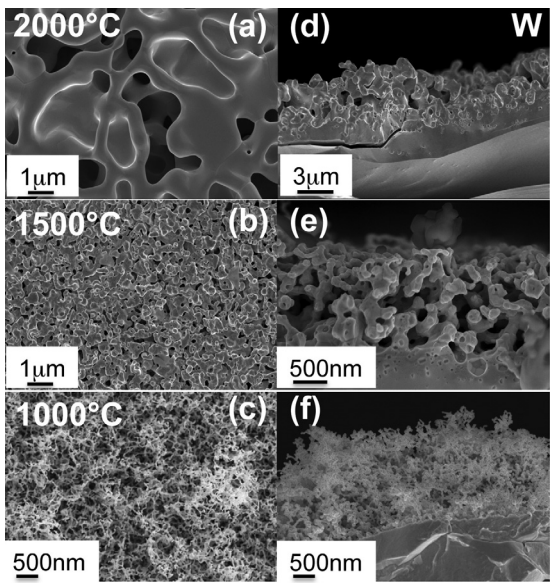

FIG. 8. Evolution of the helium-induced surface morphology changes of tungsten surfaces as a function of the surface temperature during plasma exposure ($E_{ion} = 45$ eV). For each temperature, top-views and cross-sections are shown on the left and right sides, respectively. The exposure duration was 1000 s for the samples prepared at 1500 °C and 2000 °C, and 500 s for the sample prepared at 1000 °C.

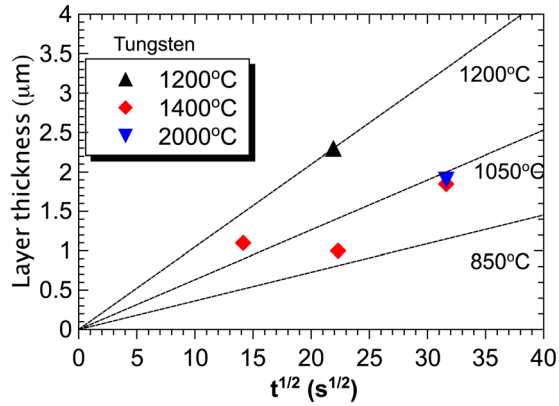

FIG. 9. (Color online) Evolution of the thickness of the nanostructured region as a function of exposure time for tungsten surfaces, with $E_{ion} = 45$ eV.

In contrast to the case of molybdenum surfaces, the kinetic development of helium-induced nanostructures has been previously studied by Baldwin and Doerner.[6] for temperatures of 850 °C and 1050 °C. The thickness of the nanostructured layer was found to follow a Fick's law (*i.e.*, $d\ t^{1/2}$) with an activation energy of 0.71 eV. A similar relationship was established by Kajita *et al.*[21] for slightly higher surface temperatures (1130 °C). The latter study, however, concluded to an effective diffusion coefficient which is actually intermediate between the values derived at 850 °C and 1050 °C in Ref. 6. It should be mentioned that in those two references, the plasma exposure is made in a single step while the results in this study have been obtained with successive plasma exposures with a duration of 100 s—the surface morphologies being actually similar in the three different studies.

The temporal evolution of the nanostructured layers produced on tungsten in this study is plotted in Fig. 9 for three different surface temperatures—corresponding to the samples shown in Fig. 8. In order to compare the present results with previously reported data, the measured structure thickness is reported as a function of $t^{1/2}$. The dashed lines represent the growth rate observed in Ref. 6 for the cases of 850 °C and 1050 °C (experimentally measured), while an extrapolation to 1200 °C of these results assuming the

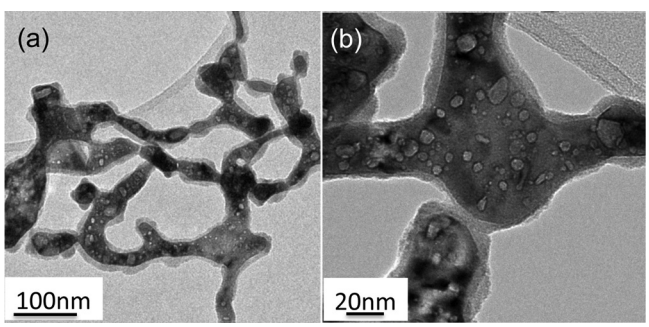

FIG. 10. Transmission electron microscope images of tungsten filaments formed on a tungsten surface during helium plasma exposure. The surface was exposed at 1000 °C for 500 s with $E_{ion} = 45$ eV. (a) and (b) are images of the same area with different magnifications.

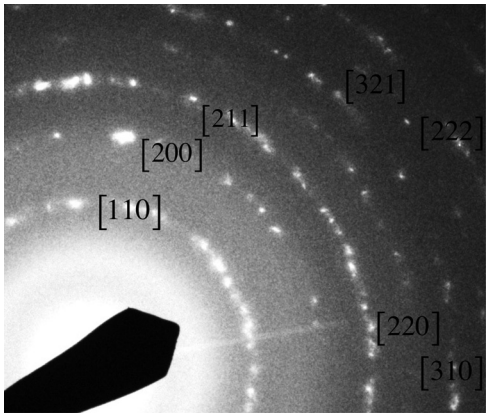

FIG. 11. Electron diffraction pattern of the tungsten filaments with hkl identification.

measured activation energy of 0.71 eV is also plotted. The measured nanostructure thickness at 1200 °C is in good agreement with the expected thickness while significantly lower growth rates are observed at higher temperatures. For instance, the growth rate obtained for a 500 s exposure ($t^{1/2} = 22.4\ s^{1/2}$) is decreased by a factor of 2 when the surface temperature is increased from 1200 °C to 1400 °C. On the other hand, the final thickness after 1000 s of exposure is similar for temperatures of 1400 °C and 2000 °C. The exposure times in the present study are on the low side of those in Refs. 6 and 21, where up to 100 times higher exposure times are used. The restricted exposure time range might increase the observed deviation from previous results. The studies by Baldwin *et al.* have been done at temperatures below 1050 °C while the two other studies deal with surface temperature above 1200 °C. Re-crystallization of tungsten starts in the temperature range 1200 °C–1400 °C (depending on the initial grade and preparation). For temperatures above 1200 °C, the reported growth rates are lower than that at 1050 °C and below. At the same time, however, the void size increases strongly with temperature which has been described in Ref. 22 albeit in the temperature range 730 °C–1160 °C. Also, studies of desorption of implanted helium from tungsten surfaces have shown the presence of desorption peaks at 730 °C, 1230 °C, and 1930 °C,[17,23] There is therefore an interplay between helium bubble formation, coalescence, re-crystallization, and desorption influencing the final surface structure.

Transmission electron microscopy (TEM) was used to gain more insight into the inner structure of the tungsten filaments. Figure 10 shows TEM pictures of tungsten filaments collected from the surface of a plasma-exposed tungsten sample exposed at 1000 °C for a duration of 500 s (fluence $= 3.2 \times 10^{26} m^{-2}$). The arborescent nature of the nanostructure is evident from Fig. 10(a). A large number of nanometric bubbles can be observed inside the filaments [Fig. 10(b)] with a wide size distribution and sizes lower than 20 nm. The voids present irregular shapes with faceted structures. No spherical voids can be observed. The interference patterns between the transmitted and diffracted electron beams reveal the presence of parallel atomic planes in the filament core, indicating a crystalline structure (Fig. 11). The structure is similar to that of α-tungsten, which is the stable form of tungsten.

IV. CONCLUSIONS

Our results show that nanostructure formation on molybdenum and tungsten by low energy helium ions proceeds along the same scheme and depends on similar experimental parameters, namely the ion energy, surface temperature, and exposure time. The size of the resulting structure is mostly dependent on the surface temperature which is thus the most critical parameter for the control of the filament size and structure porosity. It has previously been demonstrated[15] that structures similar to those shown in Figs. 8(c) and 8(f) had a reflectance lower than 1% across the visible spectrum. The results presented here show that the formation of such highly porous structures can be realized on both molybdenum and tungsten surfaces by low-energy helium ion irradiation.

[1]R. van de Krol, Y. Liang, and J. Schoonman, J. Mater. Chem. **18**, 2311 (2008).
[2]J. Su, L. Guo, N. Bao, and A. C. Grimes, Nano Lett. **11**, 1928 (2011).
[3]E. Rephaeli and S. Fan, Appl. Phys. Lett. **92**, 211107 (2008).
[4]K. Tokunaga, M. J. Baldwin, R. P. Doerner, N. Noda, Y. Kubota, N. Yoshida, T. Sogabe, T. Kato, and B. Schedler, J. Nucl. Mater. **337–339**, 887 (2005).
[5]S. Takamura, N. Ohno, D. Nishijima, and S. Kajita, J. Plasma Fusion Res. **1**, 51 (2006).
[6]M. J. Baldwin and R. P. Doerner, Nucl. Fusion **48**, 035001 (2008)
[7]S. Kajita, W. Sakaguchi, N. Ohno, N. Yoshida, and T. Saeki, Nucl. Fusion **49**, 095005 (2009).
[8]S. I. Krasheninnikov, Phys. Scr., T **145**, 014040 (2011)
[9]M. J. Baldwin and R. P. Doerner, J. Nucl. Mater. **404**, 165 (2010).
[10]S. Kajita, T. Saeki, Y. Hirahata, and N. Ohno, Jpn. J. Appl. Phys. **50**, 01AH02 (2011)
[11]G. J. van Rooij *et al.*, Appl. Phys. Lett. **90**, 121501 (2007).
[12]H. J. van der Meiden *et al.*, Rev. Sci. Instrum. **79**, 013505 (2008).
[13]P. C. Stangeby, *The Plasma Boundary of Magnetic Fusion Devices* (Institute of Physics Publishing, Bristol and Philadelphia, 2002).
[14]M. A. van den Berg, K. Bystrov, R. Pasquet, J. J. Zielinski, and G. De Temmerman, "Thermographic determination of the sheath heat transmission coefficients in a high density plasma," J. Nucl. Mater. (submitted).
[15]S. Kajita, T. Saeki, N. Yoshida, N. Ohno, and A. Iwamae, Appl. Phys. Express **3**, 085204 (2011).
[16]W. Sakaguchi, S. Kajita, N. Ohno, and M. Takagi, J. Nucl. Mater. **390–391**, 1149 (2009).
[17]M. J. Baldwin, T. C. Lynch, R. P. Doerner, and J. H. Yu, J. Nucl. Mater. **415**, S104 (2011).
[18]K. O. E. Henriksson, K. Nordlund, and J. Keinonen, Nucl. Instrum. Methods Phys. Res. B **244**, 377 (2006).
[19]K. J. Close and J. Yarwood, Br. J. Appl. Phys. **18**, 1593 (1967)
[20]M. J. Baldwin, R. P. Doerner, D. Nishijima, K. Tokunaga, and Y. Ueda, J. Nucl. Mater. **390–391**, 886 (2009).
[21]S. Kajita, N. Yoshida, R. Yoshihara, N. Ohno, and M. Yamagiwa, J. Nucl. Mater. **418**, 152 (2011).
[22]S. Sharafat, A. Takahashi, Q. Hu, and N. M. Ghoniem, J. Nucl. Mater. **386–388**, 900 (2009).
[23]E. V. Kornelsen and A. A. van Gorkum, J. Nucl. Mater. **92**, 79 (1980).